LA-UR-20-27610
Accepted Manuscript

Natural gas maximal load delivery for multi-contingency analysis

Tasseff, Byron Alexander
Coffrin, Carleton James
Bent, Russell Whitford
Sundar, Kaarthik
Zlotnik, Anatoly V.

Provided by the author(s) and the Los Alamos National Laboratory (2022-10-28).

To be published in: Computers & Chemical Engineering

DOI to publisher's version: 10.1016/j.compchemeng.2022.108032

Permalink to record:
http://permalink.lanl.gov/object/view?what=info:lanl-repo/lareport/LA-UR-20-27610

Journal Pre-proof

Natural gas maximal load delivery for multi-contingency analysis

Byron Tasseff, Carleton Coffrin, Russell Bent, Kaarthik Sundar, Anatoly Zlotnik

PII: S0098-1354(22)00366-0
DOI: https://doi.org/10.1016/j.compchemeng.2022.108032
Reference: CACE 108032

To appear in: *Computers and Chemical Engineering*

Received date : 16 April 2022
Revised date : 31 July 2022
Accepted date : 2 October 2022

Please cite this article as: B. Tasseff, C. Coffrin, R. Bent et al., Natural gas maximal load delivery for multi-contingency analysis. *Computers and Chemical Engineering* (2022), doi: https://doi.org/10.1016/j.compchemeng.2022.108032.

Natural Gas Maximal Load Delivery for Multi-contingency Analysis

Byron Tasseff*, Carleton Coffrin, Russell Bent, Kaarthik Sundar, Anatoly Zlotnik

Los Alamos National Laboratory, Los Alamos, New Mexico, USA

Abstract

An increasing dependence on natural gas has amplified existing vulnerabilities to the power grid, including disruptions to gas transmission networks from natural and man-made disasters. To address the operational challenges arising from these disruptions, we consider the problem of estimating the steady-state operating capacity of a damaged gas pipeline network while ensuring the maximal delivery of load. Specifically, we formulate the mixed-integer nonconvex maximal load delivery (MLD) problem, which proves difficult to solve on large-scale networks. To address this challenge, we present a relaxation of the MLD problem and use it to determine bounds on the transport capacity of a gas pipeline system. A rigorous computational evaluation over network models ranging in size from 11 to 4,197 junctions shows that the relaxation-based method is suitable for analyzing the impacts of multi-contingency network disruptions, often converging to the optimal solution of the relaxation in less than ten seconds.

Keywords: convex relaxation, multi-contingency, natural gas, network

Nomenclature

Sets

$\mathcal{N}$	Set of junctions (nodes)
$\mathcal{R}$	Set of receipts (producers)
$\mathcal{D}$	Set of deliveries (consumers)
$\mathcal{A}$	Set of junction-connecting components
$\mathcal{P} \subset \mathcal{A}$	Set of horizontal pipes

*Corresponding author.
Email address: byron@tasseff.com (Byron Tasseff)

$\mathcal{S} \subset \mathcal{A}$	Set of short pipes
$\mathcal{T} \subset \mathcal{A}$	Set of resistors
$\mathcal{U} \subset \mathcal{A}$	Set of constant loss resistors
$\mathcal{V} \subset \mathcal{A}$	Set of valves
$\mathcal{W} \subset \mathcal{A}$	Set of pressure-reducing regulators
$\mathcal{C} \subset \mathcal{A}$	Set of compressors
$\delta_i^+ \subset \mathcal{A}$	Set of junction-connecting components directed *from* $i \in \mathcal{N}$
$\delta_i^- \subset \mathcal{A}$	Set of junction-connecting components directed *to* $i \in \mathcal{N}$

Parameters

$\underline{p}_i, \overline{p}_i \geq 0$	Lower, upper pressure bounds for $i \in \mathcal{N}$
$\underline{\pi}_i, \overline{\pi}_i \geq 0$	Lower, upper squared pressure bounds for $i \in \mathcal{N}$
$\underline{f}_{ij}, \overline{f}_{ij} \in \mathbb{R}$	Lower, upper mass flow bounds for $(i, j) \in \mathcal{A}$
$\overline{s}_i \geq 0$	Upper supply mass flow bound for $i \in \mathcal{R}$
$\overline{d}_i \geq 0$	Upper demand mass flow bound for $i \in \mathcal{D}$
$w_{ij} \geq 0$	Resistance of pipe $(i, j) \in \mathcal{P}$
$\tau_{ij} \geq 0$	Resistance of resistor $(i, j) \in \mathcal{T}$
$\xi_{ij} \geq 0$	Pressure loss magnitude across constant loss resistor $(i, j) \in \mathcal{U}$
$\underline{\alpha}_{ij}, \overline{\alpha}_{ij} \geq 0$	Lower, upper scalars for $(i, j) \in \mathcal{W} \cup \mathcal{C}$
$\beta_i \geq 0$	Load restoration priority for delivery $i \in \mathcal{D}$

Variables

$p_i \geq 0$	Pressure at junction $i \in \mathcal{N}$
$\pi_i \geq 0$	Squared pressure at junction $i \in \mathcal{N}$
$f_{ij} \in \mathbb{R}$	Mass flow along $(i, j) \in \mathcal{A}$
$z_{ij} \in \{0, 1\}$	Status of controllable element $(i, j) \in \mathcal{V} \cup \mathcal{W}$
$y_{ij} \in \{0, 1\}$	Flow direction along $(i, j) \in \mathcal{A}$
$s_i \geq 0$	Supply at receipt $i \in \mathcal{R}$
$d_i \geq 0$	Demand at delivery $i \in \mathcal{D}$
$\ell_{ij} \geq 0$	Squared pressure loss across pipe $(i, j) \in \mathcal{P}$

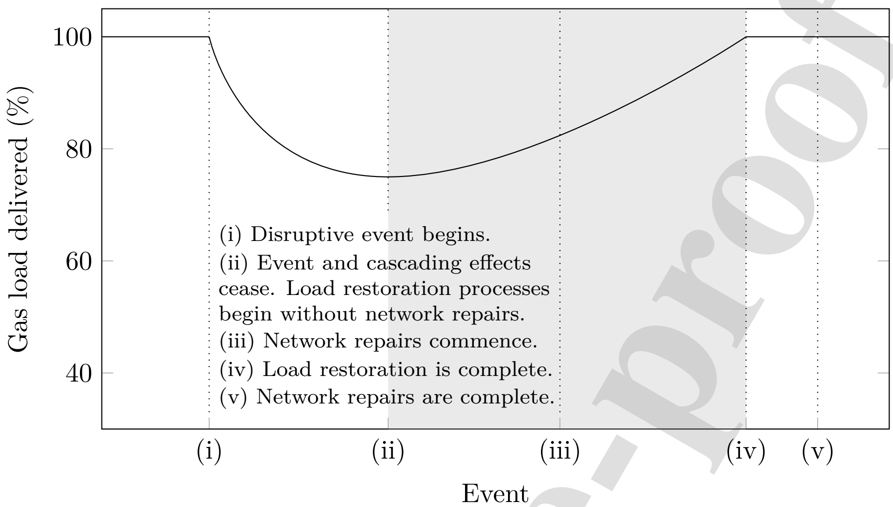

Figure 1: Illustration of a natural gas network's response to a severe disruption. The shaded region indicates the points in the disruption and restoration timeline that are examined in this study using an optimization-based assessment of damaged natural gas network capacities.

1. Introduction

Globally, electricity generation capacity is expected to grow from 21.6 trillion kilowatt-hours (kWh) in 2012 to 36.5 trillion kWh in 2040. Of this capacity, generation from natural gas is expected to grow from 22% to 28% (Conti et al., 2016). This growing dependence underscores the susceptibility of power systems to upstream disruptions in gas transmission networks. The most recent example of this trend is the February 2021 Texas power crisis, where the Electric Reliability Council of Texas experienced a loss of nearly 52.3 GW (48.6%) of its generation capacity. Nearly half of this loss was attributed to a lack of gas-fired power generation (ERCOT, 2021). Another example is the 2014 polar vortex, where curtailments in gas delivery resulted in roughly 25% of generation outages throughout the Pennsylvania-New Jersey-Maryland Interconnection (PJM Interconnection, 2014). Aside from downstream effects on the power grid, these disruptions inhibit the transport of fuel for residential heating, which provides temperature control to many individual homes during winter months. Mitigating the effects of these disruptions is critical to the resilience of gas and power delivery networks. To that end, this study examines how to estimate the transport capacity of a gas pipeline network during a large-scale disruption, whose origin (e.g., a natural hazard or sophisticated attack) is treated agnostically.

The scope of the response measures considered in this study is illustrated at a high level in Figure 1. When a hazard event begins, (i) delivery of load decreases as gas network components are damaged, cascading effects begin, and existing linepack in operational pipelines begin to deplete; and (ii) cascading effects cease, and a new stable operating point is found. After (ii), some amount of load can be restored through operational methods until (iii) network repairs commence. These repairs are conducted in accord with other restoration processes until (iv) all load can be delivered. Repairs continue until (v) all network components are operational. Addressing the complete scope of Figure 1 is a substantial and complex task. In this study, we focus specifically on estimating optimal steady-state operating capacities between events of types (ii) and (iv), which would result from operational decisions that enable the delivery of a maximal amount of load in a damaged gas pipeline network.

Several commercial tools exist for analyzing the operation of gas pipelines in the steady-state and transient regimes, including the NextGen pipeline simulation suite (Gregg Engineering, 2021), Energy Solutions' gas management software (Energy Solutions, 2021), and Atmos Pipe (Atmos International, 2021). These tools are designed for capacity planners to simulate the operation of a gas pipeline network under various physical conditions and flow nominations rather than for resilience analysis. When one or more components are assumed to be nonoperational (e.g., to simulate damage caused by a natural disaster) and must be removed from the network model, this must typically be done manually in such tools. Thus, evaluating the impact of many thousands of multi-component outage scenarios using existing tools is too labor-intensive to be practical. Furthermore, because some deliveries (demand) and receipts (supply) may need to be adjusted (or omitted) because of component outages, a new feasible operating solution, including flow allocation and compressor settings, must be quickly obtained for each scenario. It is therefore unclear how existing tools can be used for probabilistic risk assessment in this setting. This motivates a mathematical approach that can determine a feasible natural gas pipeline operating point that maximizes delivery subject to the multi-contingency damage considerations.

In this study, we formalize this task as the steady-state Maximal Load Delivery (MLD) problem. Informally, the problem is stated as follows: given a severely damaged gas pipeline network in which a number of components have become nonoperational, we maximize the amount of prioritized load that can be served in the damaged network subject to steady-state pipeline physical flow, capacity limits, pressure bounds, and other operating requirements. The nonlinear physics of gas transport and the discrete nature of operations in the network (i.e., the opening and closing of valves) render this problem a challenging mixed-integer nonlinear, nonconvex program. To address this, we introduce a mixed-integer convex relaxation of the MLD problem, which is found to be a reliable means for estimating the upper bound of maximum deliverable load.

Recent interest in large-scale gas network planning and control has led to a wide variety of optimization-based applications and methodologies. Hiller et al. (2018) provide a summary of studies connected to the optimization-based evaluation of gas network capacities. Schmidt et al. (2016) present detailed steady-state models and approximations of network components for use in optimization applications. Hahn et al. (2017), Gugat et al. (2018), and Hoppmann-Baum et al. (2021) present mixed-integer programming approaches for optimization problems involving gas transport in the transient regime. Finally, Hante (2017,

2020) describes relaxation methods for similar mixed-integer control problems.

The methodology of this study is primarily inspired by the success of approaches developed for multi-contingency analysis of power transmission networks. A similar optimization study on damaged power grids was motivated by the analysis of natural disaster vulnerabilities (Coffrin et al., 2019). In that study, the MLD problem was formulated for alternating current (AC) power networks, and convex relaxations were developed that allow for the problem's efficient solution on large-scale instances. Another study introduced convex relaxations for gas network expansion planning (Borraz-Sánchez et al., 2016). Similar convex relaxations for gas pipeline flow have been explored subsequently (Chen et al., 2018; Wu et al., 2017). These convex relaxations largely inspire the convex reformulation of the MLD problem described in this study. Extending these studies, we present nonconvex models and convex relaxations for gas network components that were previously not explicitly considered, e.g., resistors.

A number of studies consider problems similar to the MLD developed here. Sundar et al. (2018) and Ahumada-Paras et al. (2021) examine the problems of identifying the k components of a power transmission network and gas pipeline network, respectively, whose simultaneous failure maximizes disruption to the network. Their studies use MLD problems as inner portions of broader bilevel interdiction problems. In contrast, we seek to determine an optimal operating point and estimate the network capacity for a given disruption rather than determine the worst-case disruption. Other studies have considered the classic throughput maximization problem in the context of natural gas networks, although none have considered the contingency analysis application described in this study (Arya & Honwad, 2018; Midthun et al., 2009; Misra et al., 2015). Finally, Bent et al. (2018) consider the joint expansion planning problem for gas and power networks. Their study, which links power generation to gas delivery, serves as a reference for future extensions of the methods presented in this study.

Compared to the prior literature, the contributions of our study include

- The first formulation of the steady-state MLD problem for gas networks;
- A mixed-integer nonconvex quadratic reformulation of the MLD problem;
- A tractable mixed-integer convex relaxation of the MLD problem;
- A rigorous benchmarking of the formulations on instances of various sizes;
- A proof of concept MLD analysis for spatially distributed natural hazards.

The remaining sections proceed as follows: Section 2 defines the requirements for gas pipeline operational feasibility as a mixed-integer nonconvex program; Section 3 formulates the MLD problem as a mixed-integer nonconvex program, then proposes a mixed-integer convex relaxation of the problem; Section 4 rigorously benchmarks the MLD formulations across several gas network data sets of various sizes and evaluates the use of the MLD method for probabilistic risk assessment for spatial natural hazards; and Section 5 concludes the study.

2. Background

This section presents the background for modeling natural gas transmission networks in a steady-state regime. For completeness, in Section 2.1, the transient dynamics for gas pipelines are stated, and standard physical assumptions are imposed to derive the pressure-flow equation for steady-state turbulent flow. This nonconvex equation describes the loss in potential (i.e., pressure) along each pipe as a nonlinear function of flow and represents one of the primary optimization modeling challenges addressed in subsequent sections. In Section 2.2, additional physical constraints required for network operation are described.

2.1. Pipeline Modeling Assumptions

The dynamics of gas pipeline flow are modeled via the following set of partial differential equations (PDEs) over space and time (Osiadacz, 1987):

$$\frac{\partial \phi}{\partial x} + \frac{\partial \rho}{\partial t} = 0, \tag{1a}$$

$$\frac{\partial (\phi v)}{\partial x} + \frac{\partial \phi}{\partial t} + \frac{\partial p}{\partial x} = -\frac{\lambda}{2D}\phi |v| - g \sin \alpha \rho, \tag{1b}$$

$$p - ZRT\rho = 0. \tag{1c}$$

Here, Equation (1a) represents conservation of mass, Equation (1b) represents conservation of momentum, and Equation (1c) is the equation of state that relates the pressure and density. In these PDEs, the gas mass flux ϕ, density ρ, velocity v, and pressure p evolve over both space and time, x and t, respectively. In Equation (1b), λ denotes the friction factor of the pipe and, unless given, is computed via an explicit approximation of the Colebrook-White equation for turbulent flow. This approximation is derived as (Zeghadnia et al., 2019)

$$\lambda = \left[2 \log \left(\frac{3.7D}{\epsilon} \right) \right]^{-2}, \tag{2}$$

where D denotes the diameter of the pipe wall and ϵ denotes the absolute pipe roughness (in units of length). Additionally, in Equations (1b) and (1c), g denotes acceleration due to gravity, α denotes the angle of inclination of the pipe with respect to the horizontal, Z denotes the gas compressibility factor, T denotes the temperature of the gas, and R denotes the universal gas constant. While in practice, the gas compressibility, Z, depends significantly on pressure and temperature in the regime of high pressure gas pipeline flow, in this study, we assume an ideal equation of state and suppose Z and T to be fixed, as often done to explore new concepts in similar academic studies (Schmidt et al., 2016).

We assume all pipes are level, which allows the gravitational term of Equation (1b) to be ignored. We also assume the temperature T is constant along a pipe. Finally, we assume the system has reached a steady state, and all time derivatives vanish. With these assumptions, Equation (1a) reduces to $\partial_x \phi = 0$. Equation (1b), after imposing assumptions and multiplying by ρ, reduces to

$$p\frac{\partial p}{\partial x} = -\frac{ZR\lambda T}{2D}\phi|\phi| \implies \frac{\partial p^2}{\partial x} = -\frac{ZR\lambda T}{D}\phi|\phi|. \tag{3}$$

Finally, integrating Equation (3) from zero to the length of the pipe, L, gives

$$[p(0)]^2 - [p(L)]^2 = \gamma\phi|\phi| \implies [p(L)]^2 - [p(0)]^2 = -\gamma\phi|\phi|, \tag{4}$$

where the pipe's resistance term is defined via the relation $\gamma := \frac{ZLR\lambda T}{D}$. Equation (4) is referred to as the pressure-flow equation for turbulent flow, and its nonconvex form presents a critical challenge for optimization applications.

We remark that, although less accurate than a transient model, we consider our use of a steady-state model justified for this contingency analysis application. As emphasized by Figure 1, our study does not consider the transient events that immediately follow a network disruption. More specifically, the goal of the MLD is to estimate how much load can be delivered at or after point (ii) in this figure, i.e., the point at which all remedial actions and resources, such as linepack, have been exhausted. This task is thus equivalent to computing the maximum capacity (or throughput) of the (degraded) network and is determinable using a steady-state model. Note that steady-state assumptions are standard in mid- to long-term capacity planning tasks (Koch et al., 2015).

2.2. Network Modeling

Aside from pipes, gas networks include a variety of other components (Koch et al., 2015), each of which is modeled using different sets of variables and constraints. This subsection describes the nonconvex models of all components.

Notation for Sets. A natural gas transmission network is represented by a graph $\mathcal{G} := (\mathcal{N}, \mathcal{A})$, where $\mathcal{N}$ is the set of junctions (nodes) and $\mathcal{A}$ is the set of node-connecting components (arcs). The set of receipts (producers) is denoted by $\mathcal{R}$ and deliveries (consumers) by $\mathcal{D}$. Receipts and deliveries are attached to existing junctions $i \in \mathcal{N}$. Furthermore, we let the subset of receipts attached to $i \in \mathcal{N}$ be denoted by $\mathcal{R}_i$ and the subset of deliveries by $\mathcal{D}_i$. The sets of horizontal and short pipes in the network are denoted by $\mathcal{P} \subset \mathcal{A}$ and $\mathcal{S} \subset \mathcal{A}$, respectively; the set of regular and constant loss resistors by $\mathcal{T} \subset \mathcal{A}$ and $\mathcal{U} \subset \mathcal{A}$, respectively; the set of valves and regulating (i.e., control) valves by $\mathcal{V} \subset \mathcal{A}$ and $\mathcal{W} \subset \mathcal{A}$, respectively; and the set of compressors by $\mathcal{C} \subset \mathcal{A}$. Finally, the set of node-connecting components incident to junction $i \in \mathcal{N}$ where i is the tail (respectively, head) of the arc is denoted by $\delta_i^+ := \{(i,j) \in \mathcal{A}\}$ (respectively, $\delta_i^- := \{(j,i) \in \mathcal{A}\}$). We next examine each of the aforementioned components individually, define the decision variables, and present constraints that each component enforces on the gas network's operations. In particular, for each component, we present two types of constraints: (i) operational limits and (ii) physical constraints. We start by examining junctions of the network.

Junctions. Each junction $i \in \mathcal{N}$ in the network is associated with a pressure variable, p_i. Operational limits require that this pressure resides between predefined lower and upper bounds, denoted by $\underline{p}_i$ and $\overline{p}_i$, respectively, i.e.,

$$0 \leq \underline{p}_i \leq p_i \leq \overline{p}_i, \forall i \in \mathcal{N}. \tag{5}$$

We note that for a subset of predefined "slack junctions" $\mathcal{N}^s \subset \mathcal{N}$, $\underline{p}_i = \overline{p}_i$.

Node-connecting Components. Every node-connecting component $(i, j) \in \mathcal{A}$ is associated with a decision variable, f_{ij}, which denotes the mass flow rate across that component. These variables must first satisfy the capacity constraints

$$\underline{f}_{ij} \leq f_{ij} \leq \overline{f}_{ij},\ \forall (i, j) \in \mathcal{A}. \tag{6}$$

Unlike a directed graph, flow for each $(i, j) \in \mathcal{A}$ can be nonnegative *or* negative. A nonnegative (respectively, negative) value of f_{ij} implies mass flow that is directed from node i to j (respectively, j to i). Furthermore, for a pipe $(i, j) \in \mathcal{P}$, mass flow f_{ij} and mass flux ϕ_{ij} are related by $f_{ij} := \frac{\pi}{4} D_{ij}^2 \phi_{ij}$. In the forthcoming paragraphs, we present the constraints required for modeling the operational limits and physics of all node-connecting components in the gas network.

Pipes. Pipes are the primary means for transporting gas throughout a pipeline network. In steady-state flow, each pipe satisfies the pressure-flow Equation (4), which relates the mass flow rate f_{ij} through the cross-sectional area of the pipe to the pressures p_i and p_j at the two end-points of the pipe. That is,

$$p_i^2 - p_j^2 = w_{ij} f_{ij} |f_{ij}|,\ \forall (i, j) \in \mathcal{P}, \tag{7}$$

where the mass flow resistance w_{ij} is related to γ_{ij} via $w_{ij} := (16\gamma_{ij})/(\pi^2 D_{ij}^4)$.

Short Pipes. Short pipes are components that model resistanceless transport of flow between two junctions. This is equivalent to treating the length term of a pipe's resistance as negligible. Short pipes thus ensure the equality of pressures at the two junctions, i and j, connected by that component, i.e.,

$$p_i - p_j = 0,\ \forall (i, j) \in \mathcal{S}. \tag{8}$$

Resistors. Aside from pressure losses that arise from the pressure-flow equation, a variety of other phenomena can also induce pressure loss. Examples include turbulence in shaped components, effects of measurement devices, curvature of piping, and partially closed valves. Resistors serve as surrogate modeling tools for representing these other forms of pressure loss. Losses across resistors are modeled using the Darcy-Weisbach-inspired equations (Koch et al., 2015)

$$p_i - p_j = \tau_{ij} f_{ij} |f_{ij}|,\ \forall (i, j) \in \mathcal{T}. \tag{9}$$

Here, the resistance is defined by $\tau_{ij} := (8\kappa_{ij})/(\pi^2 D_{ij}^4 \rho_s)$, where κ_{ij} is the resistor's unitless drag factor, D_{ij} is the resistor's diameter, which may be artificial, and ρ_s is the average standard density of gas throughout the network. Note that, like Constraints (7), Constraints (9) are also nonconvex and nonlinear.

Loss Resistors. Loss resistors serve as an alternate form of resistors, where instead of satisfying the Darcy-Weisbach equation, a fixed pressure loss $\xi_{ij} \geq 0$ is incurred across the component (Koch et al., 2015). Modeling these pressure losses for all loss resistors requires imposing the constraints

$$f_{ij}(p_i - p_j) \geq 0,\ \forall (i, j) \in \mathcal{U} \tag{10a}$$

$$(p_i - p_j)^2 = \xi_{ij}^2,\ \forall (i, j) \in \mathcal{U}. \tag{10b}$$

Here, Constraints (10a) ensure that the mass flow across each loss resistor is in the direction of the pressure loss, and each Constraint (10b) relates the pressure loss magnitude ξ_{ij} across the loss resistor to the difference of pressures.

Valves. Valves are used to route the flow of gas to certain portions of the network or to block flow during maintenance of subnetworks. In this study, valves are controllable elements that are either closed or open. In practice, valves can be partially closed to control the gas velocity, but in these cases, we choose to model the valve as a resistor (Koch et al., 2015). The operating status of each valve $(i, j) \in \mathcal{V}$ is indicated using a binary variable $z_{ij} \in \{0, 1\}$, where $z_{ij} = 1$ corresponds to an open valve and $z_{ij} = 0$ to a closed valve. These variables disjunctively constrain the mass flow across each valve as

$$\underline{f}_{ij} z_{ij} \leq f_{ij} \leq \overline{f}_{ij} z_{ij},\ z_{ij} \in \{0, 1\},\ \forall (i, j) \in \mathcal{V}. \tag{11}$$

Furthermore, when a valve is open, the pressures at the junctions connected by that valve are equal. When the valve is closed, these pressures are decoupled. This phenomenon is modeled via the following set of disjunctive constraints:

$$p_i \leq p_j + (1 - z_{ij})\overline{p}_i,\ \forall (i, j) \in \mathcal{V} \tag{12a}$$
$$p_j \leq p_i + (1 - z_{ij})\overline{p}_j,\ \forall (i, j) \in \mathcal{V}. \tag{12b}$$

Regulators. Large pipes are usually operated at higher pressures than other portions of the network. As such, interconnection of large pipes with smaller pipes often requires the use of pressure regulators (i.e., control valves) to reduce pressure between differently-sized pipes. Regulators can also be used as an additional means of controlling flow throughout the network (Koch et al., 2015). The operating status of a regulator is modeled using a binary variable $z_{ij} \in \{0, 1\}$, where $z_{ij} = 1$ and $z_{ij} = 0$ indicate active and inactive statuses, respectively. The mass flow across each regulator is then governed by

$$\underline{f}_{ij} z_{ij} \leq f_{ij} \leq \overline{f}_{ij} z_{ij},\ z_{ij} \in \{0, 1\},\ \forall (i, j) \in \mathcal{W}. \tag{13}$$

Furthermore, each regulator (i, j) is associated with a multiplicative scaling factor, α_{ij}, that defines the relationship between p_i and p_j when the regulator is active, i.e., $\alpha_{ij} p_i = p_j$. This factor is constrained by operating limits as $\underline{\alpha}_{ij} = 0 \leq \alpha_{ij} \leq \overline{\alpha}_{ij} = 1$. As for valves, the pressures at the junctions connected by a regulator are decoupled when the regulator is inactive. This is modeled by

$$f_{ij}(p_i - p_j) \geq 0,\ \forall (i, j) \in \mathcal{W} \tag{14a}$$
$$\underline{\alpha}_{ij} p_i \leq p_j + (1 - z_{ij})\underline{\alpha}_{ij}\overline{p}_i,\ \forall (i, j) \in \mathcal{W} \tag{14b}$$
$$p_j \leq \overline{\alpha}_{ij} p_i + (1 - z_{ij})\overline{p}_j,\ \forall (i, j) \in \mathcal{W}. \tag{14c}$$

Here, Constraints (14a) ensure that each mass flow is in the same direction as the pressure loss, while Constraints (14b) and (14c) ensure the pressure at node j resides within the scaled bounds of p_i when the control valve is open.

Compressors. Each compressor $(i,j) \in \mathcal{C}$ boosts the pressure at the downstream junction $j \in \mathcal{N}$ by a variable scalar α_{ij} and is assumed to have negligible length. For the networks considered in this paper, compressors permitting bidirectional compression do not appear, although each compressor may or may not allow for *uncompressed* flow in the reverse direction, i.e., from j to i. These distinct behaviors of compressors are captured by three conditional sets of constraints.

The first set of constraints describes the behavior of compressors where uncompressed reverse flow is prohibited. These constraints are presented as

$$\underline{\alpha}_{ij} p_i \leq p_j \leq \overline{\alpha}_{ij} p_i, \; \forall (i,j) \in \mathcal{C} : \underline{f}_{ij} \geq 0, \tag{15}$$

where $\underline{\alpha}_{ij}$ and $\overline{\alpha}_{ij}$, $(i,j) \in \mathcal{C}$, are minimum and maximum compression ratios.

The second set of constraints describes the behavior of compressors where reverse flow *is* allowed and the minimum compression ratio is equal to one:

$$\underline{\alpha}_{ij} p_i \leq p_j \leq \overline{\alpha}_{ij} p_i, \; \forall (i,j) \in \mathcal{C} : \underline{f}_{ij} < 0 \land \underline{\alpha}_{ij} = 1 \tag{16a}$$

$$f_{ij}(p_i - p_j) \leq 0, \; \forall (i,j) \in \mathcal{C} : \underline{f}_{ij} < 0 \land \underline{\alpha}_{ij} = 1. \tag{16b}$$

Here, Constraints (16b) ensure that, if $f_{ij} < 0$ (i.e., when there exists reverse flow), then $p_i = p_j$ (i.e., there is no change in pressure across the compressor).

The final set of constraints describes the behavior of compressors where uncompressed reverse flow is allowed and the minimum compression ratio is *not* equal to one. In this case, the behavior of the compressor must be modeled disjunctively. To accomplish this, for each compressor, a binary variable $y_{ij} \in \{0,1\}$ is introduced to denote the direction of flow through the compressor, where $y_{ij} = 1$ implies flow from i to j and $y_{ij} = 0$ implies flow from j to i. The pressures at the junctions that connect each compressor are then modeled as

$$y_{ij} \in \{0,1\}, \; \forall (i,j) \in \mathcal{C} : \underline{f}_{ij} < 0 \land \underline{\alpha}_{ij} \neq 1 \tag{17a}$$

$$p_j \leq \overline{\alpha}_{ij} p_i + (1 - y_{ij}) \overline{p}_j, \; \forall (i,j) \in \mathcal{C} : \underline{f}_{ij} < 0 \land \underline{\alpha}_{ij} \neq 1 \tag{17b}$$

$$\underline{\alpha}_{ij} p_i \leq p_j + (1 - y_{ij}) \overline{p}_i, \; \forall (i,j) \in \mathcal{C} : \underline{f}_{ij} < 0 \land \underline{\alpha}_{ij} \neq 1 \tag{17c}$$

$$p_i - p_j \leq y_{ij} \overline{p}_i, \; \forall (i,j) \in \mathcal{C} : \underline{f}_{ij} < 0 \land \underline{\alpha}_{ij} \neq 1 \tag{17d}$$

$$p_j - p_i \leq y_{ij} \overline{p}_j, \; \forall (i,j) \in \mathcal{C} : \underline{f}_{ij} < 0 \land \underline{\alpha}_{ij} \neq 1. \tag{17e}$$

Here, Constraints (17b) and (17c) ensure that, when a compressor's flow is positively directed, the pressure at node j is modeled according to the compression ratio bounds. Constraints (17d) and (17e) ensure that, when flow is reversed (i.e., $y_{ij} = 0$), the pressures on both sides of the compressor are equal.

Receipts, Deliveries, and Mass Conservation. Receipts and deliveries are points in the network that are attached to junctions where gas can be supplied to and withdrawn from the network, respectively. Each receipt (respectively, delivery) is associated with a nonnegative constant $\overline{s}_k$ (respectively, $\overline{d}_k$) that denotes the fixed mass supply (respectively, demand) at receipt $k \in \mathcal{R}$ (respectively, delivery $k \in \mathcal{D}$). Mass conservation throughout the network then requires nodal flow balance constraints to be enforced at every junction. These constraints are stated as

$$\sum_{(i,j)\in\delta_i^+} f_{ij} - \sum_{(j,i)\in\delta_i^-} f_{ji} = \sum_{k\in\mathcal{R}_i} \overline{s}_k - \sum_{k\in\mathcal{D}_i} \overline{d}_k, \; \forall i \in \mathcal{N}. \tag{18}$$

Feasibility Problem. Given the constraints that model each component in the gas network, the nonconvex program for steady-state feasibility is thus

Pressure/mass flow bounds	Constraints (5), (6)	
Pipe modeling	Constraints (7)	
Short pipe modeling	Constraints (8)	
Resistor modeling	Constraints (9)	
Loss resistor modeling	Constraints (10)	(MINCP-F)
Valve modeling	Constraints (11), (12)	
Regulator modeling	Constraints (13), (14)	
Compressor modeling	Constraints (15), (16), (17)	
Mass conservation	Constraints (18).	

The goal of (MINCP-F) is to determine if gas can be routed through the pipeline network while satisfying the operational limits and physical constraints imposed by each component of the network. As formulated, the problem is a mixed-integer nonconvex program. The nonconvexities of the system of equations (MINCP-F) arise from three sources: (i) the discreteness of controllable components; (ii) bilinear products of variables appearing in flow direction-related inequalities, i.e., Constraints (10a), (14a), and (16b); and (iii) nonlinear equations, i.e., Constraints (7), (9), and (10b). Section 3 first describes a mixed-integer nonconvex quadratic reformulation of this system that addresses (ii) and reformulates the nonconvex disjunctive behavior of (iii), followed by a mixed-integer convex quadratic relaxation that addresses the remaining nonconvexities of (iii).

3. Maximal Load Delivery Formulations

This section formulates the MLD problem, which seeks to estimate the transport capacity of a damaged gas pipeline network while ensuring the maximal delivery of prioritized load. To the best of our knowledge, this is the first time such a problem has been formulated for gas networks. Three variants of the problem are presented in order of successive reformulations and relaxations that, though they increase the number of constraints, decrease nonlinear nonconvexity and, generally, computational difficulty. First, Section 3.1 extends the nonconvex feasibility constraints of (MINCP-F) to formulate the initial MLD problem. Section 3.2 introduces an *exact* mixed-integer nonconvex quadratic reformulation of this problem. To alleviate the challenges associated with nonconvexity, a mixed-integer convex quadratic *relaxation* is derived in Section 3.3.

Aside from formulating the MLD problem, compared to previous studies (e.g., Ahumada-Paras et al., 2021; Bent et al., 2018; Borraz-Sánchez et al., 2016; Chen et al., 2018; Wu et al., 2017), this section also (i) presents mixed-integer quadratic reformulations for a broader set of gas pipeline network components and (ii) introduces convex relaxation techniques for components that were not explicitly considered in these prior studies (e.g., resistors and loss resistors).

3.1. Mixed-integer Nonconvex Formulation

A damaged gas network requires the exclusion of components from the model described in Section 2.2. This set of excluded components comprises both the damaged components themselves as well as any connected components. For example, a damaged junction $i \in \mathcal{N}$ implies a nonoperational status of all node-connecting components $\delta_i^+ \cup \delta_i^-$. To this end, we introduce a tilde-based notation to define the sets of components that are *still functional* within a damaged gas network, e.g., $\widetilde{\mathcal{P}} \subseteq \mathcal{P}$ denotes the set of pipes that are still operational.

The fundamental motivation for formulating the MLD problem is that a damaged gas network may not be able to satisfy all demands of the original system. This implies a possible imbalance of the mass conservation Constraints (18). To address this, in the MLD problem, all receipts and deliveries are treated as dispatchable (or variable). This implies the previous constant supplies and demands, $\overline{s}_k$, $k \in \mathcal{R}_i$, and $\overline{d}_k$, $k \in \mathcal{D}_i$, for $i \in \mathcal{N}$, become variables bounded as

$$0 \leq s_k \leq \overline{s}_k, \forall k \in \mathcal{R}_i, \; \forall i \in \widetilde{\mathcal{N}} \tag{19a}$$

$$0 \leq d_k \leq \overline{d}_k, \forall k \in \mathcal{D}_i, \; \forall i \in \widetilde{\mathcal{N}}, \tag{19b}$$

where $\overline{s}_k$ and $\overline{d}_k$ denote the original supplies and demands, respectively. Using these variable loads, the previous mass conservation Constraints (18) become

$$\sum_{(i,j) \in \widetilde{\delta}_i^+} f_{ij} - \sum_{(j,i) \in \widetilde{\delta}_i^-} f_{ji} = \sum_{k \in \mathcal{R}_i} s_k - \sum_{k \in \mathcal{D}_i} d_k, \; \forall i \in \widetilde{\mathcal{N}}. \tag{20}$$

Next, parameters $\beta_k \geq 0$, $k \in \mathcal{D}$, are introduced to denote load restoration priorities. If no load priorities are available, values of one can be used instead. (Indeed, this parameterization is used for all of our experiments in Section 4.) Maximization of prioritized load delivered then implies the objective function

$$\eta(d) = \sum_{i \in \widetilde{\mathcal{N}}} \sum_{k \in \mathcal{D}_i} \beta_k d_k. \tag{21}$$

The mixed-integer nonconvex MLD problem formulation is then

maximize	Objective function	$\eta(d)$ of Equation (21)	(MINCP)
subject to	Supply/demand bounds	Constraints (19)	
	Mass conservation	Constraints (20)	
	Physical feasibility	(MINCP-F) $\setminus$ {Cons. (18)},	

where in (MINCP-F), all component sets are replaced with their tilde-denoted counterparts to indicate the application of a network damage scenario.

3.2. Mixed-integer Nonconvex Quadratic Reformulation

As summarized at the end of Section 2.2, one source of nonconvexity in (MINCP) is the disjunctive behavior of nonlinear equations involving products of flow with its absolute value, i.e., Constraints (7) and (9). These disjunctions arise from the lack of a priori knowledge concerning flow directionality throughout the network, which can change based on operational decisions. In this section, we first employ a standard mathematical programming rewriting of these disjunctive constraints, which involves the introduction of binary direction variables, $y_{ij} \in \{0, 1\}$ for all $(i, j) \in \widetilde{\mathcal{A}}$. Second, this section introduces squared pressure variables, $\pi_i = p_i^2$ for all $i \in \widetilde{\mathcal{N}}$, which further linearize Constraints (7).

We remark that, although this reformulation introduces new nonconvexities via discrete elements, it removes the *implied* nonconvex disjunctions of Constraints (7) and (9). This provides an *exact* mixed-integer nonconvex quadratic reformulation of the original problem. That is, the new reformulation contains fewer continuous nonlinearities than (MINCP) but has the same solution set. This new formulation enables *global* solutions to be found with modern commercial mixed-integer quadratic programming solvers (namely, Gurobi). Further, because the reformulation is based on flow direction, intuitive topology- and direction-based inequalities are available to improve the formulation's scalability, as is done later in this subsection. Later, in Section 3.3, this formulation is relaxed to form a mixed-integer *convex* quadratic relaxation of the MLD.

Junctions. Squared pressures must reside between predefined bounds, i.e.,

$$\underline{\pi}_i \leq \pi_i \leq \overline{\pi}_i, \forall i \in \widetilde{\mathcal{N}}. \tag{22}$$

where $\underline{\pi}_i$ and $\overline{\pi}_i$, $i \in \widetilde{\mathcal{N}}$, are derived from the bounds $\underline{p}_i$ and $\overline{p}_i$, respectively.

Node-connecting Components. Using the binary flow direction variables, the mass flow bounds of all node-connecting components are restricted as

$$(1 - y_{ij})\underline{f}_{ij} \leq f_{ij} \leq y_{ij}\overline{f}_{ij},\ y_{ij} \in \{0, 1\},\ \forall (i, j) \in \widetilde{\mathcal{A}}. \tag{23}$$

Pipes. Squared pressure variables and directions allow for the reduction of nonlinearities in the pressure-flow Constraints (7) for pipes, rewritten here as

$$\pi_i - \pi_j \geq w_{ij} f_{ij}^2 - (1 - y_{ij}) \left[w_{ij} \underline{f}_{ij}^2 - (\underline{\pi}_i - \overline{\pi}_j) \right], \forall (i, j) \in \widetilde{\mathcal{P}} \tag{24a}$$

$$\pi_i - \pi_j \leq w_{ij} f_{ij}^2, \forall (i, j) \in \widetilde{\mathcal{P}} \tag{24b}$$

$$\pi_j - \pi_i \geq w_{ij} f_{ij}^2 - y_{ij} \left[w_{ij} \overline{f}_{ij}^2 - (\underline{\pi}_j - \overline{\pi}_i) \right], \forall (i, j) \in \widetilde{\mathcal{P}} \tag{24c}$$

$$\pi_j - \pi_i \leq w_{ij} f_{ij}^2, \forall (i, j) \in \widetilde{\mathcal{P}}. \tag{24d}$$

This is similar to the reformulation presented by Borraz-Sánchez et al. (2016). Here, each Constraint (24a) ensures nonincreasing pressure from i to j when $y_{ij} = 1$ (nonnegative flow). Constraint (24b) ensures the pressure-flow equation is satisfied when $y_{ij} = 1$. Constraint (24c) ensures nonincreasing pressure from

j to i when $y_{ij} = 0$. Constraint (24d) ensures the pressure-flow equation is satisfied when $y_{ij} = 0$. Directions are used to strengthen Constraints (24) via

$$(1 - y_{ij})(\underline{\pi}_i - \overline{\pi}_j) \leq \pi_i - \pi_j,\ \forall (i,j) \in \widetilde{\mathcal{P}} \tag{25a}$$

$$\pi_i - \pi_j \leq y_{ij}(\overline{\pi}_i - \underline{\pi}_j),\ \forall (i,j) \in \widetilde{\mathcal{P}}. \tag{25b}$$

Short Pipes. Squared pressures allow for rewriting Constraints (8) as

$$\pi_i - \pi_j = 0,\ \forall (i,j) \in \widetilde{\mathcal{S}}. \tag{26}$$

As with pipes, direction variables are used to bound squared pressures via

$$(1 - y_{ij})(\underline{\pi}_i - \overline{\pi}_j) \leq \pi_i - \pi_j,\ \forall (i,j) \in \widetilde{\mathcal{S}} \tag{27a}$$

$$\pi_i - \pi_j \leq y_{ij}(\overline{\pi}_i - \underline{\pi}_j),\ \forall (i,j) \in \widetilde{\mathcal{S}}. \tag{27b}$$

Resistors. For junctions that are connected to a resistor, the squared pressure variables π_i, $i \in \widetilde{\mathcal{N}}$, must be related to variables denoting pressure, i.e.,

$$p_i^2 - \pi_i = 0,\ i \in \widetilde{\mathcal{N}} : \left(\exists (i,j) \in \widetilde{\mathcal{T}}\right) \vee \left(\exists (j,i) \in \widetilde{\mathcal{T}}\right). \tag{28}$$

The potential loss is then written in a manner as for that of pipes, i.e.,

$$p_i - p_j \geq w_{ij} f_{ij}^2 - (1 - y_{ij}) \left[w_{ij} \underline{f}_{ij}^2 - (\underline{p}_i - \overline{p}_j) \right],\ \forall (i,j) \in \widetilde{\mathcal{T}} \tag{29a}$$

$$p_i - p_j \leq w_{ij} f_{ij}^2,\ \forall (i,j) \in \widetilde{\mathcal{T}} \tag{29b}$$

$$p_j - p_i \geq w_{ij} f_{ij}^2 - y_{ij} \left[w_{ij} \overline{f}_{ij}^2 - (\underline{p}_j - \overline{p}_i) \right],\ \forall (i,j) \in \widetilde{\mathcal{T}} \tag{29c}$$

$$p_j - p_i \leq w_{ij} f_{ij}^2,\ \forall (i,j) \in \widetilde{\mathcal{T}}, \tag{29d}$$

Direction variables are also used to bound the original pressure variables via

$$(1 - y_{ij})(\underline{p}_i - \overline{p}_j) \leq p_i - p_j,\ \forall (i,j) \in \widetilde{\mathcal{T}} \tag{30a}$$

$$p_i - p_j \leq y_{ij}(\overline{p}_i - \underline{p}_j),\ \forall (i,j) \in \widetilde{\mathcal{T}}. \tag{30b}$$

Loss Resistors. As for resistors, squared pressure variables π_i, $i \in \widetilde{\mathcal{N}}$, for junctions connected to a loss resistor, must be related to pressure variables via

$$p_i^2 - \pi_i = 0,\ i \in \widetilde{\mathcal{N}} : \left(\exists (i,j) \in \widetilde{\mathcal{U}}\right) \vee \left(\exists (j,i) \in \widetilde{\mathcal{U}}\right). \tag{31}$$

Note that Constraints (10) can be rewritten using absolute values as

$$\xi_{ij} = |p_i - p_j|,\ \forall (i,j) \in \widetilde{\mathcal{U}}. \tag{32}$$

However, directions y_{ij} allow this disjunctive form to be modeled linearly, i.e.,

$$(2y_{ij} - 1)\xi_{ij} = p_i - p_j,\ \forall (i,j) \in \widetilde{\mathcal{U}}. \tag{33}$$

Here, the direction of pressure loss coincides with the direction given by y_{ij}.

Valves. Pressure Constraints (12) are written with squared pressures as

$$\pi_i \leq \pi_j + (1 - z_{ij})\overline{\pi}_i,\ \forall (i,j) \in \widetilde{\mathcal{V}} \tag{34a}$$
$$\pi_j \leq \pi_i + (1 - z_{ij})\overline{\pi}_j,\ \forall (i,j) \in \widetilde{\mathcal{V}}. \tag{34b}$$

Regulators. Pressure Constraints (14) are written with squared pressures as

$$\pi_j - \overline{\alpha}_{ij}^2\pi_i \leq (2 - y_{ij} - z_{ij})\overline{\pi}_j,\ \forall (i,j) \in \widetilde{\mathcal{W}} \tag{35a}$$
$$\underline{\alpha}_{ij}^2\pi_i - \pi_j \leq (2 - y_{ij} - z_{ij})\overline{\pi}_i,\ \forall (i,j) \in \widetilde{\mathcal{W}} \tag{35b}$$
$$\pi_j - \pi_i \leq (1 + y_{ij} - z_{ij})\overline{\pi}_j,\ \forall (i,j) \in \widetilde{\mathcal{W}} \tag{35c}$$
$$\pi_i - \pi_j \leq (1 + y_{ij} - z_{ij})\overline{\pi}_i,\ \forall (i,j) \in \widetilde{\mathcal{W}}. \tag{35d}$$

Here, when $y_{ij} = 1$ and $z_{ij} = 1$ (i.e., the regulating valve is open and the flow direction is positive), Constraints (35a) and (35b) ensure that π_j resides between the scaled value of π_i. When $y_{ij} = 0$ and $z_{ij} = 1$, Constraints (35c) and (35d) ensure that $\pi_i = \pi_j$, and reverse flow is allowed. Finally, when the valve is closed, $z_{ij} = 0$ and $y_{ij} \in \{0, 1\}$, which ensures π_i and π_j are decoupled.

Compressors. Constraints (15), which model compressors where uncompressed reverse flow is prohibited, are written with squared pressures as

$$\underline{\alpha}_{ij}^2\pi_i \leq \pi_j \leq \overline{\alpha}_{ij}^2\pi_i,\ \forall (i,j) \in \widetilde{\mathcal{C}} : \underline{f}_{ij} \geq 0. \tag{36}$$

For compressors that allow reverse flow, Constraints (16) and (17) become

$$\pi_j \leq \overline{\alpha}_{ij}^2\pi_i + (1 - y_{ij})\overline{\pi}_j,\ \forall (i,j) \in \widetilde{\mathcal{C}} : \underline{f}_{ij} < 0 \tag{37a}$$
$$\underline{\alpha}_{ij}^2\pi_i \leq \pi_j + (1 - y_{ij})\underline{\alpha}_{ij}^2\overline{\pi}_i,\ \forall (i,j) \in \widetilde{\mathcal{C}} : \underline{f}_{ij} < 0 \tag{37b}$$
$$\pi_i - \pi_j \leq y_{ij}\overline{\pi}_i,\ \forall (i,j) \in \widetilde{\mathcal{C}} : \underline{f}_{ij} < 0 \tag{37c}$$
$$\pi_j - \pi_i \leq y_{ij}\overline{\pi}_j,\ \forall (i,j) \in \widetilde{\mathcal{C}} : \underline{f}_{ij} < 0. \tag{37d}$$

Here, when $y_{ij} = 1$, Constraints (37a) and (37b) require π_j to reside within the scaled bounds of π_i. When $y_{ij} = 0$, Constraints (37c) and (37d) ensure the equality of pressures when flow is from j to i (i.e., there is no compression).

Direction-related Valid Inequalities. The formulations of Borraz-Sánchez et al. (2016) include valid inequalities that relate node-connecting component directions y_{ij} to nodal conditions in the directed network. These inequalities improve relaxed formulations. Here, we employ the constraints that model flow directionality at junctions with zero supply, zero demand, and degree two:

$$\sum_{(j,i)\in\widetilde{\delta}_i^-} y_{ji} - \sum_{(i,j)\in\widetilde{\delta}_i^+} y_{ij} = 0,\ i \in \widetilde{\mathcal{N}}_0 : \left(\left|\widetilde{\delta}_i^{\pm}\right| = 1\right) \tag{38a}$$
$$\sum_{(j,i)\in\widetilde{\delta}_i^-} y_{ji} + \sum_{(i,j)\in\widetilde{\delta}_i^+} y_{ij} = 1,\ i \in \widetilde{\mathcal{N}}_0 : \left(\left|\widetilde{\delta}_i^{\pm}\right| = 2\right) \wedge \left(\left|\widetilde{\delta}_i^{\mp}\right| = 0\right), \tag{38b}$$

where $\widetilde{\mathcal{N}}_0 \subset \widetilde{\mathcal{N}}$ denotes the subset of junctions where $\sum_{k \in \mathcal{R}_i} \overline{s}_i = \sum_{k \in \mathcal{D}_i} \overline{d}_i = 0$. These constraints imply that, for this subset of junctions, the direction of incoming mass flow must be equal to the direction of outgoing mass flow.

Reformulation. The preceding changes enable the mixed-integer nonconvex (MINCP) to be formulated as the mixed-integer *nonconvex quadratic* program

maximize	Objective function	$\eta(d)$ of Equation (21)	
subject to	Supply/demand bounds	Constraints (19)	
	Mass conservation	Constraints (20)	
	Pressure bounds	Constraints (5), (22)	
	Directed flow bounds	Constraints (23)	
	Pipe modeling	Constraints (24), (25)	
	Short pipe modeling	Constraints (26), (27)	(MINQP)
	Resistor modeling	Constraints (28), (29), (30)	
	Loss resistor modeling	Constraints (31), (33)	
	Valve modeling	Constraints (11), (34)	
	Regulator modeling	Constraints (13), (35)	
	Compressor modeling	Constraints (36), (37)	
	Direction-related cuts	Constraints (38).	

3.3. Mixed-integer Convex Quadratic Relaxation

Convex relaxation is a popular strategy for approximating and increasing the tractability of nonconvex mathematical programming problems. The technique dates back to McCormick (1976), who described a procedure for obtaining tight convex underestimating envelopes for nonconvex functions of a single variable. In this section, we employ a similar procedure, whereby nonconvex constraints are decomposed, convexly underestimated, and linearly overestimated, which results in a *relaxation* of the original problem that *overestimates* load delivery.

There are a significant number of nonconvex nonlinear constraints in the problem (MINQP) that cause it to become computationally intractable with increasing network size. Specifically, these are Constraints (24b), (24d), (28), (29b), (29d), and (31). Here, we apply convex relaxation strategies, as done in Borraz-Sánchez et al. (2016), Wu et al. (2017), and Chen et al. (2018), to address this. We also extend these studies by formulating relaxations for components that were not previously considered, e.g., resistors and loss resistors, which require constraints involving explicit pressure variables. Most of these relaxations rely on the observation that (i) pressure-flow functions are symmetric about the origin and (ii) direction variables can serve to "activate" or "deactivate" convex envelopes of these functions, depending on the flow direction (i.e., value of y_{ij}).

Pipes. We first apply convex relaxations to the pressure-flow Constraints (24) for pipes. As previously mentioned, these relaxations serve to activate or deactivate the symmetric convex envelopes centered about a point of zero flow.

The variables ℓ_{ij} for $(i,j) \in \widetilde{\mathcal{P}}$ are introduced to denote the difference (loss) in squared pressures across each pipe. The relaxation constraints are then

$$\pi_j - \pi_i \leq \ell_{ij},\ \pi_i - \pi_j \leq \ell_{ij},\ \forall (i,j) \in \widetilde{\mathcal{P}} \tag{39a}$$

$$\ell_{ij} \leq \pi_j - \pi_i + (2y_{ij})(\overline{\pi}_i - \underline{\pi}_j),\ \forall (i,j) \in \widetilde{\mathcal{P}} \tag{39b}$$

$$\ell_{ij} \leq \pi_i - \pi_j + (2y_{ij} - 2)(\underline{\pi}_i - \overline{\pi}_j),\ \forall (i,j) \in \widetilde{\mathcal{P}} \tag{39c}$$

$$w_{ij} f_{ij}^2 \leq \ell_{ij},\ \forall (i,j) \in \widetilde{\mathcal{P}} \tag{39d}$$

$$\ell_{ij} \leq w_{ij} \overline{f}_{ij} f_{ij} + (1 - y_{ij}) \left(\left| w_{ij} \overline{f}_{ij} \underline{f}_{ij} \right| + w_{ij} \underline{f}_{ij}^2 \right),\ \forall (i,j) \in \widetilde{\mathcal{P}} \tag{39e}$$

$$\ell_{ij} \leq w_{ij} \underline{f}_{ij} f_{ij} + y_{ij} \left(\left| w_{ij} \overline{f}_{ij} \underline{f}_{ij} \right| + w_{ij} \overline{f}_{ij}^2 \right),\ \forall (i,j) \in \widetilde{\mathcal{P}}. \tag{39f}$$

Here, Constraints (39a) ensure squared pressure loss magnitudes, ℓ_{ij}, are lower-bounded by the largest nonnegative difference of squared pressures. Constraints (39b) ensure that when $y_{ij} = 0$, i.e., for negative flow, each loss magnitude is upper-bounded by (and, because of Constraints (39a), equal to) $\pi_j - \pi_i$. Constraints (39c) similarly imply that when $y_{ij} = 1$, each loss is upper-bounded by (and thus equal to) $\pi_i - \pi_j$. Observe that ℓ_{ij} will thus always be nonnegative.

Constraints (39d) are the primary convex relaxations of the pressure-flow equations. These constraints ensure that, no matter the direction of flow, each pressure loss magnitude, ℓ_{ij}, is *convexly underestimated* by the pressure-loss relationship. Finally, Constraints (39e) and (39f) apply linear upper bounds on each variable ℓ_{ij}, depending on the choice of flow direction. That is, when $y_{ij} = 1$, the loss magnitude is overestimated according to the flow's *upper bound*, and when $y_{ij} = 0$, it is overestimated according to the flow's *lower bound*.

Resistors. We next apply convex relaxations to Constraints (28), which relate nonsquared and squared pressure variables. These inequality relaxations yield

$$p_i^2 \leq \pi_i,\ i \in \widetilde{\mathcal{N}} : \left(\exists (i,j) \in \widetilde{\mathcal{T}} \right) \vee \left(\exists (j,i) \in \widetilde{\mathcal{T}} \right). \tag{40}$$

Constraints (29) are then relaxed as done for Constraints (39), i.e.,

$$p_j - p_i \leq \ell_{ij},\ p_i - p_j \leq \ell_{ij},\ \forall (i,j) \in \widetilde{\mathcal{T}} \tag{41a}$$

$$\ell_{ij} \leq p_j - p_i + (2y_{ij})(\overline{p}_i - \underline{p}_j),\ \forall (i,j) \in \widetilde{\mathcal{T}} \tag{41b}$$

$$\ell_{ij} \leq p_i - p_j + (2y_{ij} - 2)(\underline{p}_i - \overline{p}_j),\ \forall (i,j) \in \widetilde{\mathcal{T}} \tag{41c}$$

$$w_{ij} f_{ij}^2 \leq \ell_{ij},\ \forall (i,j) \in \widetilde{\mathcal{T}} \tag{41d}$$

$$\ell_{ij} \leq w_{ij} \overline{f}_{ij} f_{ij} + (1 - y_{ij}) \left(\left| w_{ij} \overline{f}_{ij} \underline{f}_{ij} \right| + w_{ij} \underline{f}_{ij}^2 \right),\ \forall (i,j) \in \widetilde{\mathcal{T}} \tag{41e}$$

$$\ell_{ij} \leq w_{ij} \underline{f}_{ij} f_{ij} + y_{ij} \left(\left| w_{ij} \overline{f}_{ij} \underline{f}_{ij} \right| + w_{ij} \overline{f}_{ij}^2 \right),\ \forall (i,j) \in \widetilde{\mathcal{T}}. \tag{41f}$$

Loss Resistors. As we have done for resistors, we apply convex relaxations to Constraints (31) relating nonsquared and squared pressures. We obtain

$$p_i^2 \leq \pi_i, \; i \in \widetilde{\mathcal{N}} : \left(\exists (i,j) \in \widetilde{\mathcal{U}}\right) \vee \left(\exists (j,i) \in \widetilde{\mathcal{U}}\right). \tag{42}$$

Relaxation. The mixed-integer convex quadratic relaxation of (MINQP) is

maximize	Objective function	$\eta(d)$ of Equation (21)	
subject to	Supply/demand bounds	Constraints (19)	
	Mass conservation	Constraints (20)	
	Pressure bounds	Constraints (5), (22)	
	Directed flow bounds	Constraints (23)	
	Pipe dynamics	Constraints (25), (39)	
	Short pipe dynamics	Constraints (26), (27)	(MICQP)
	Resistor dynamics	Constraints (30), (40), (41)	
	Loss resistor dynamics	Constraints (33), (42)	
	Valve dynamics	Constraints (11), (34)	
	Regulator dynamics	Constraints (13), (35)	
	Compressor dynamics	Constraints (36), (37)	
	Direction-related cuts	Constraints (38).	

In Section 4, we present the results of a comprehensive computational study performed to compare the tractability and application of the exact and relaxed MLD problem formulations, (MINQP) and (MICQP), respectively. These computations display the practical benefits of employing the relaxation, (MICQP).

4. Computational Experiments

This section experimentally analyzes the applicability and computational performance of the (MINQP) and (MICQP) MLD formulations presented in Section 3. This informs the practical, analytical, and computational trade-offs associated with using the exact and relaxed MLD problem formulations, respectively. To accomplish this, we consider three different types of damage scenarios: (i) $N-1$ or single contingency scenarios, (ii) $N-k$ or multi-contingency scenarios, and (iii) earthquake damage scenarios. Each scenario is intended to simulate common sources of damage to a gas pipeline network. Although these damage models arise from physically reasonable assumptions, we do not claim to quantify the robustness of the specific networks considered. Rather, these models serve as proofs of concept for studying three aspects of the MLD problem: (i) understanding the tractability of MLD formulations, (ii) highlighting the qualitative insights given by an MLD analysis, and (iii) providing guidelines for future applications of this work to real-world network disruption scenarios.

Both MLD formulations are implemented in the Julia programming language using the mathematical modeling layer JuMP, version 0.21 (Dunning

Network	$\lvert\mathcal{N}\rvert$	$\lvert\mathcal{P}\rvert$	$\lvert\mathcal{S}\rvert$	$\lvert\mathcal{T}\rvert$	$\lvert\mathcal{U}\rvert$	$\lvert\mathcal{V}\rvert$	$\lvert\mathcal{W}\rvert$	$\lvert\mathcal{C}\rvert$
`GasLib-11`	11	8	0	0	0	1	0	2
`Belgian-20`	20	24	0	0	0	0	0	3
`GasLib-24`	24	19	1	1	0	0	1	3
`GasLib-40`	40	39	0	0	0	0	0	6
`GasLib-134`	134	86	45	0	0	0	1	1
`GasLib-135`	135	141	0	0	0	0	0	29
`NA-154`	154	140	0	0	0	0	0	12
`GasLib-582`	582	278	269	8	0	26	23	5
`GasLib-4197`	4197	3537	343	22	6	426	120	12

Table 1: Summary of natural gas transmission networks derived from open data.

et al., 2017), and version 0.8 of GasModels, an open-source Julia package for steady-state and transient natural gas network optimization (Bent et al., 2022). Section 4.1 describes the instances, computational resources, and parameters used throughout these experiments; Section 4.2 compares the efficacy of MLD formulations on $N-1$ contingency scenarios for each network; Section 4.3 does the same for randomized $N-k$ multi-contingency scenarios, where k corresponds to 15% of node-connecting components in each network; and Section 4.4 compares the runtime performance of the formulations over both the $N-1$ and $N-k$ experiment sets. Section 4.5 provides a proof-of-concept application of the MLD problem to damage scenarios precipitated by deterministic or stochastic spatially distributed natural hazards (in this case, earthquakes). Finally, Section 4.6 examines the feasibility of relaxation-based (MICQP) integer solutions when fixed within the nonrelaxed (MINQP) MLD formulation.

4.1. Experimental Test Data & Setup

The numerical experiments consider realistic networks of various sizes that appear in literature of natural gas transmission network modeling or are derivable from open data. These instances are summarized in Table 1. Here, the `Belgium-20` network is derived from the application of De Wolf & Smeers (2000); the North American 154-junction network (i.e., `NA-154`) is derived by subject matter experts using public data; and `GasLib` networks are obtained directly from Schmidt et al. (2017). For the `GasLib-582` and `GasLib-4197` networks, the `nomination_freezing_1` and `nomination_mild_0006` delivery and receipt nominations are used, respectively. Generally, steady-state optimization problems involving most networks can be solved to optimality given a small amount of time (e.g., seconds to minutes). The notable exception is the `GasLib-4197` network, the largest system, which requires hours to solve many instances.

Each optimization computation was provided a wall-clock time of one hour on a node containing two Intel Xeon E5-2695 v4 processors, each with 18 cores at 2.10 GHz, and 125 GB of memory. For solutions of the nonconvex and convex MIQPs, Gurobi 9.0 was used with the parameter `MIPGap=0.0`. For experiments

	MINQP			MICQP		
Network	Opt. (%)	Lim. (%)	Inf. (%)	Opt. (%)	Lim. (%)	Inf. (%)
`GasLib-11`	100.0	0.0	0.0	100.0	0.0	0.0
`Belgium-20`	100.0	0.0	0.0	100.0	0.0	0.0
`GasLib-24`	100.0	0.0	0.0	100.0	0.0	0.0
`GasLib-40`	100.0	0.0	0.0	100.0	0.0	0.0
`GasLib-134`	100.0	0.0	0.0	100.0	0.0	0.0
`GasLib-135`	90.2	9.8	0.0	100.0	0.0	0.0
`NA-154`	100.0	0.0	0.0	100.0	0.0	0.0
`GasLib-582`	79.6	20.4	0.0	100.0	0.0	0.0
`GasLib-4197`	3.2	90.3	6.5	43.8	56.2	0.0

Table 2: Comparison of solver termination statuses over all $N-1$ contingency scenarios. Here, "Opt." corresponds to instances where optimality was proven, "Lim." to instances where the time limit was reached, and "Inf." to instances that were claimed by the solver to be infeasible.

employing (MINQP), the setting `NonConvex=2` was used, which allows for global optimization of this formulation via Gurobi's spatial branching capabilities.

4.2. Single Contingency Damage Scenarios

The first damage model considered is the single contingency or $N-1$ model, where N corresponds to the original number of network components and $N-1$ indicates that an individual component is removed (or damaged). This model is a method for simulating the effects of a single unscheduled component outage. Here, both nodal components (i.e., junctions) and node-connecting components (e.g., pipes) can comprise a single $N-1$ damage scenario. This damage model demonstrates feasibility of the MLD problem for a variety of topologies and is used to validate our network modeling assumptions for damaged gas networks.

For each network, the set of all such possible $N-1$ scenarios was considered, and the corresponding instances were solved using both the (MINQP) and (MICQP) MLD formulations. The exception is `GasLib-4197`, which was limited to 1,040 unique scenarios because of cluster restrictions. Table 2 displays statistics of solver termination statuses across all scenarios for each network and formulation. For all networks except `GasLib-135`, `GasLib-582`, and `GasLib-4197`, optimal solutions to all instances were found within the prescribed one hour time limit. For `GasLib-135`, the (MINQP) formulation was unable to prove global optimality on 98 instances. Notably, `GasLib-135` contains the largest number of compressors compared to other networks, and these additional degrees of freedom are a primary source of computational complexity. For `GasLib-582` and `GasLib-4197`, the large number of (MINQP) instances that could not be solved to global optimality was likely because of the networks' relatively large sizes.

Comparing the two formulations shows the benefit of using the relaxation-based (MICQP) approach, which is capable of solving much larger proportions of challenging `GasLib-135`, `GasLib-582`, and `GasLib-4197` instances. This suggests that (MICQP), when compared to the mixed-integer nonconvex (MINQP), is often a better candidate for numerically intensive applications. We also note that, when using the default Gurobi parameters described in Section 4.1, 292

	MINQP			MICQP		
Network	Opt. (%)	Lim. (%)	Inf. (%)	Opt. (%)	Lim. (%)	Inf. (%)
`GasLib-11`	100.0	0.0	0.0	100.0	0.0	0.0
`Belgium-20`	100.0	0.0	0.0	100.0	0.0	0.0
`GasLib-24`	100.0	0.0	0.0	100.0	0.0	0.0
`GasLib-40`	100.0	0.0	0.0	100.0	0.0	0.0
`GasLib-134`	100.0	0.0	0.0	100.0	0.0	0.0
`GasLib-135`	99.6	0.4	0.0	100.0	0.0	0.0
`NA-154`	100.0	0.0	0.0	100.0	0.0	0.0
`GasLib-582`	99.9	0.1	0.0	100.0	0.0	0.0
`GasLib-4197`	92.7	7.3	0.0	99.2	0.8	0.0

Table 3: Comparison of termination statuses over 1,000 randomized $N-k$ multi-contingency scenarios, where k corresponds to 15% of all node-connecting components in the network.

of 1,040 `GasLib-4197` instances of the (MINQP) MLD formulation are claimed to be infeasible. Using the parameter `NumericFocus=3` for this subset of 292 instances, however, decreases this number to 68. These claimed infeasibilities are likely related to the numerical properties of the `GasLib-4197` data set rather than our MLD formulations. Additional future work to preprocess data and rescale MLD formulation constraints and nondimensionalize the formulation is warranted to address these issues.

4.3. Multi-contingency Damage Scenarios

The second damage model is the multi-contingency or $N-k$ model, where k corresponds to the number of components that are simultaneously removed from the network. These scenarios are intended to simulate the effects of multi-modal network failures. Here, we consider the removal of only node-connecting components within the generated $N-k$ scenarios. In each scenario, a uniformly random selection of 15% node-connecting components are assumed to be non-operational. Heuristically, this proportion of components seems to generate challenging MLD instances while providing different maximal load distributions across the networks considered. For each network, one thousand such scenarios were generated. If solved, the maximal proportional load delivered in each experiment was computed as the ratio of the optimal nonprioritized objective in Equation (21) and the maximal deliverable load within the *undamaged* network.

Table 3 displays statistics of solver termination statuses across all damage scenarios for each network and formulation. For all except `GasLib-135`, `GasLib-582`, and `GasLib-4197`, globally optimal solutions to MLD instances were found within the one hour time limit. For `GasLib-135` and `GasLib-582`, the (MINQP) formulation was unable to prove optimality on four instances and one instance, respectively. For `GasLib-4197`, a larger proportion could not be solved. Comparing the two formulations again shows the benefit of the relaxation-based approach, which solves larger proportions of challenging instances. We note that one `GasLib-4197` (MINQP) instance was claimed to be infeasible using default Gurobi parameters but feasible with `NumericFocus=3`.

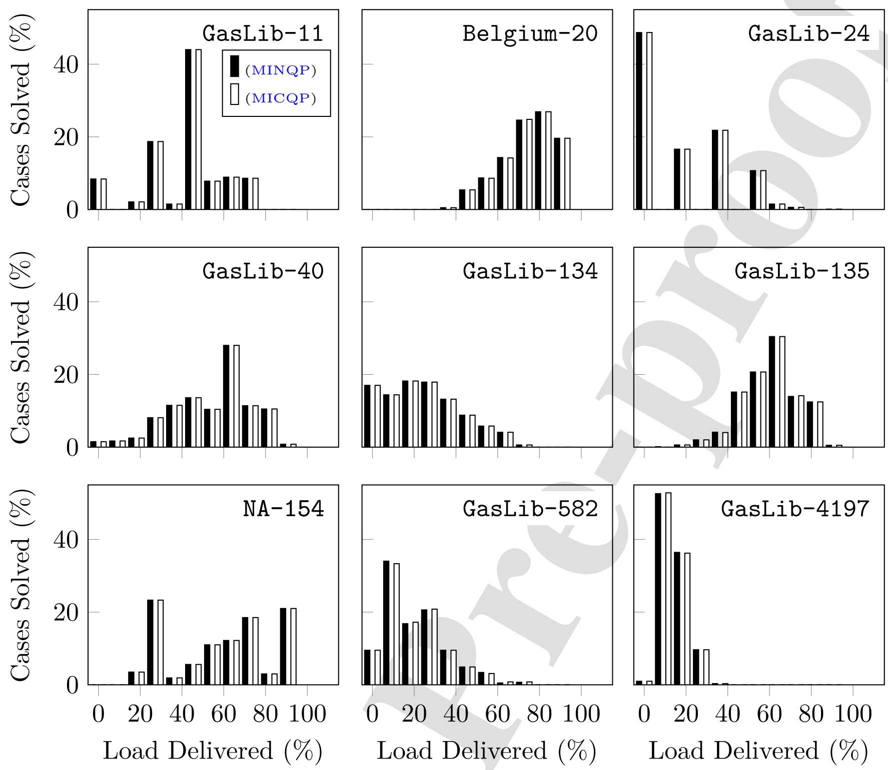

Figure 2: Histograms of load delivered over randomized $N-k$ multi-contingency scenarios using the (MINQP) and (MICQP) formulations, where k corresponds to 15% of all edges. Note that each pair of histograms summarizes instances solved by *both* (MINQP) and (MICQP).

Figure 2 displays nine histograms that compare the proportion of load delivered across *solved* damage scenarios for each network while using the two formulations. Most importantly, these histograms display the similarity of load estimates achieved while using the relaxation-based formulation. These results also indicate substantial qualitative differences in the hypothetical robustness of each network. For example, larger networks like `GasLib-582` and `GasLib-4197` are shown to be highly sensitive to the 15% damage scenarios, where often only 10% to 30% of load can be delivered. The `Belgium-20` network appears less vulnerable and is often capable of serving between 70% and 100% of the load under severe contingencies. Finally, for some smaller networks (e.g., `GasLib-11`, `GasLib-24`, `GasLib-134`), many scenarios result in zero or nearly zero maximum deliverable load. This simple analysis shows the utility of the MLD problem for understanding broad characteristics of natural gas network robustness.

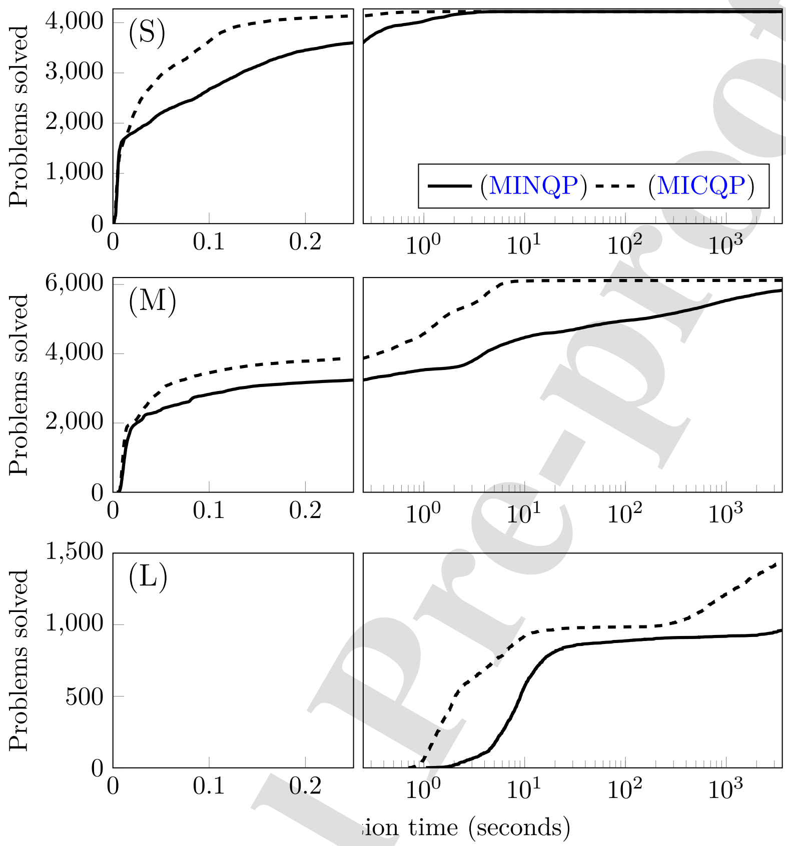

Figure 3: Performance profiles comparing the efficiency of (MINQP) and (MICQP) formulations over the instances described in Sections 4.2 and 4.3. Here, the performance profiles are divided into three categories for (S) networks containing tens of nodes; (M) networks containing hundreds of nodes; and (L) networks containing thousands of nodes (i.e., `GasLib-4197`).

4.4. Computational Performance

This section compares the performance of (MINQP) and (MICQP) MLD formulations using the benchmark instances described in Sections 4.2 and 4.3. The performance profiles for these instances are shown in Figure 3 and divided into three categories: (S) networks containing tens of nodes; (M) networks containing hundreds of nodes; and (L) networks containing thousands of nodes (i.e., `GasLib-4197`). In all such categories, it is shown that the (MICQP) formulation is able to solve substantially greater numbers of problems than (MINQP) in shorter amounts of time. For networks with tens of nodes, both formulations are capable of solving all instances in less than ten seconds. For networks with hundreds of nodes, (MICQP) is capable of solving most instances within ten seconds, while (MINQP) requires hundreds or thousands of seconds. For networks with thousands of nodes, (MICQP) solves a much greater number of instances within the alotted hour time limit, although solve times are much longer when compared with problems that consider networks of tens or hundreds of nodes.

4.5. Synthetic Earthquake Damage Scenarios

This subsection provides a proof-of-concept application to demonstrate the use of the MLD problem in the context of risk assessment for deterministic and uncertain spatial hazards. In each scenario, damage to a network is caused by an earthquake with a fixed magnitude and epicenter. For an earthquake, the probability of damage to a pipeline component is commonly represented as a function of peak ground acceleration (PGA) and peak ground velocity (PGV). These relationships for PGA and PGV are typically expressed as functions of earthquake magnitude and distance from seismographic rupture. In our study, the relationships derived by Campbell (1997) are employed, and their details are omitted here for brevity. For simplicity, we assume that all earthquakes arise from strike-slip faulting at a depth of one kilometer in a region of firm soil.

Given the PGA and PGV at a component's point in space, the vulnerability of the component is then modeled using the fragility approach of Lanzano et al. (2014) for continuous pipelines in the presence of strong ground shaking. Specifically, the probability of damage is computed as a function of PGV, and node-connecting components exceeding the damage threshold for the first risk state ("very limited loss") are assumed to be nonoperational. Again, for the purpose of brevity, these relationships are omitted here. For simplicity, we make three additional assumptions in our model: (i) only node-connecting components are affected by PGA and PGV; (ii) all node-connecting components assume the fragility curve for "continuous pipelines," and (iii) the distance from the earthquake's epicenter to each node-connecting component is the minimum distance between the epicenter and the locations of the connecting junctions.

The networks `Belgium-20`, `GasLib-40`, `GasLib-135`, `NA-154`, `GasLib-582`, and `GasLib-4197` are considered for earthquake damage scenarios, as the remaining three networks do not contain geolocation data for components.[1] Figure 4 depicts three illustrations relevant to the parameterization of scenarios.

Deterministic Earthquake, Stochastic Fragility Scenarios. The first set of earthquake scenarios demonstrates the applicability of the MLD method when analyzing network vulnerability to a known (i.e., deterministic) spatially distributed natural hazard. To this end, one earthquake was considered per network, each described by a fixed magnitude and epicenter. This type of scenario is illustrated pictorially in the first image of Figure 4. The local magnitude of each earthquake was assumed to be 8.0, while each epicenter was assumed to be the center of a k-means cluster containing the largest number of junctions, where $k = 5$. Then, using the PGV model of Campbell (1997) and the probabilistic fragility

[1] We remark that many of the example networks considered in this study are not geolocated in areas associated with high seismic risk. The goal of these results is to show how an actual analysis is conducted when the approach is applied to an area with high seismic activity.

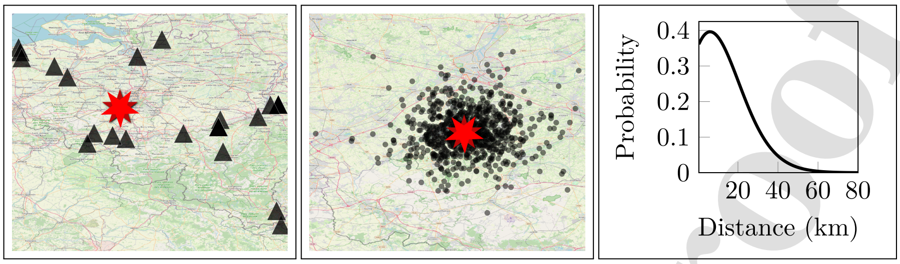

Figure 4: Illustrations of the earthquake scenarios. The first (left) shows the position of an earthquake epicenter (red star) for the `Belgium-20` network and its spatial relation to network junctions (black triangles). The second illustration (center) shows the placement of a mean earthquake epicenter (red star) for the `Belgium-20` network and random, normally distributed epicenters surrounding it (black circles). The last (right) shows an example fragility curve derived from Campbell (1997) and Lanzano et al. (2014) for a magnitude 8.0 earthquake.

	MINQP			MICQP		
Network	Opt. (%)	Lim. (%)	Inf. (%)	Opt. (%)	Lim. (%)	Inf. (%)
`Belgium-20`	100.0	0.0	0.0	100.0	0.0	0.0
`GasLib-40`	100.0	0.0	0.0	100.0	0.0	0.0
`GasLib-135`	98.3	1.7	0.0	100.0	0.0	0.0
`NA-154`	100.0	0.0	0.0	100.0	0.0	0.0
`GasLib-582`	58.7	41.3	0.0	99.8	0.2	0.0
`GasLib-4197`	2.9	95.3	1.8	86.0	14.0	0.0

Table 4: Comparison of solution statuses over the set of deterministic earthquake scenarios.

approach of Lanzano et al. (2014), one thousand damage scenarios were generated per network, where in each, the operational status per node-connecting component was determined via a uniform random sampling and comparison with the probability of damage. An example fragility curve is depicted in the rightmost image of Figure 4, which relates a component's distance from the epicenter of a magnitude 8.0 earthquake to the probability of damage.

Table 4 displays statistics of solver statuses across all damage scenarios for each network and formulation. For all except the `GasLib-135`, `GasLib-582`, and `GasLib-4197` networks, optimal solutions to instances were found within the one hour time limit. For `GasLib-135`, the (MINQP) formulation was unable to prove optimality on 17 instances. For `GasLib-582` and `GasLib-4197`, a larger proportion of (MINQP) instances could not be solved within the time limit. Even for the convex relaxation, two instances could not be solved for the `GasLib-582` network. Nonetheless, comparing the (MINQP) and (MICQP) formulations shows the benefit of the relaxation-based approach, which is capable of solving a larger proportion of instances. We note that 96 of the thousand `GasLib-4197` (MINQP) instances were claimed to be infeasible using default Gurobi parameters. This number was reduced to 18 using `NumericFocus=3`.

Figure 5 displays boxplots comparing the maximal proportion of load delivered across *solved* damage scenarios for each network and formulation. Here,

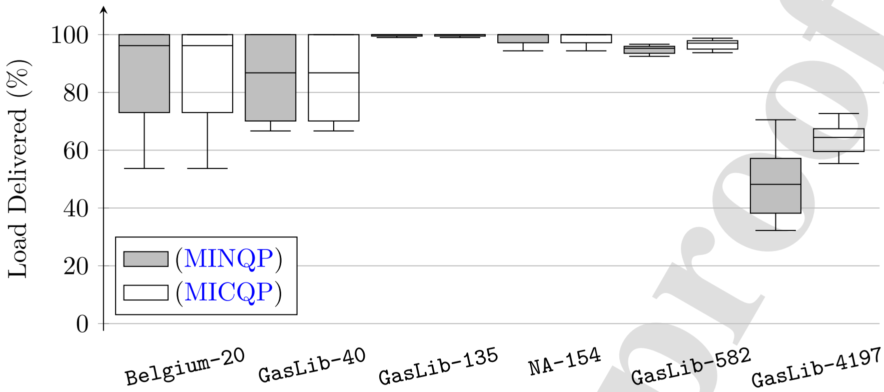

Figure 5: Boxplots of load delivered over *solved* earthquake damage scenarios per network, where the magnitude and epicenter for each network were assumed to be fixed. Note that each pair of boxplots summarizes only instances solved by *both* (MINQP) and (MICQP).

results obtained using the (MINQP) and (MICQP) formulations of the MLD problem are shown to be remarkably similar. This demonstrates the utility of the relaxation-based approach, which provides outcomes comparable to the mixed-integer nonconvex formulation at a smaller computational cost. The boxplots also show substantial qualitative differences in the (hypothetical) vulnerability among networks. For example, the `GasLib-40` network is shown to have great variability in maximal load delivered, while `GasLib-135`, `NA-154`, and `GasLib-582` are mostly unaffected by the hypothetical hazard. Additionally, some networks (e.g., `NA-154`, `GasLib-582`) predict small ranges of load delivered, while others (e.g., `Belgium-20`) appear to carry greater uncertainty.

The large discrepancies in boxplots for the `GasLib-4197` damage scenarios likely originate from two sources. First, the pair of boxplots is representative of only the subset of instances solved by *both* formulations, which is relatively small. Second, however, are the mathematical differences in nonconvex and relaxed formulations. Notably, the minima across the solvable instances differ by around twenty percent. This could be a consequence of the relaxation, which theoretically predicts maximal load values greater than or equal to the nonconvex formulation. Compared to other networks, these larger discrepancies in predicted deliverable load could be a manifestation of the component relaxations, whose errors are further aggregated as the network size grows.

Stochastic Earthquake, Stochastic Fragility Scenarios. The second set of earthquake scenarios demonstrates the applicability of the MLD method when analyzing network vulnerability to a stochastic (i.e., uncertain) natural hazard. To this end, multiple earthquakes were considered per network, where each was randomly sampled assuming normally distributed magnitudes and epicenters. This situation is illustrated in the second image of Figure 4. Here, the mean

Network	MINQP			MICQP		
	Opt. (%)	Lim. (%)	Inf. (%)	Opt. (%)	Lim. (%)	Inf. (%)
`Belgium-20`	100.0	0.0	0.0	100.0	0.0	0.0
`GasLib-40`	100.0	0.0	0.0	100.0	0.0	0.0
`GasLib-135`	97.3	2.7	0.0	100.0	0.0	0.0
`NA-154`	100.0	0.0	0.0	100.0	0.0	0.0
`GasLib-582`	97.1	2.9	0.0	100.0	0.0	0.0
`GasLib-4197`	4.4	89.7	5.9	82.8	17.2	0.0

Table 5: Comparison of termination statuses over the second set of earthquake scenarios.

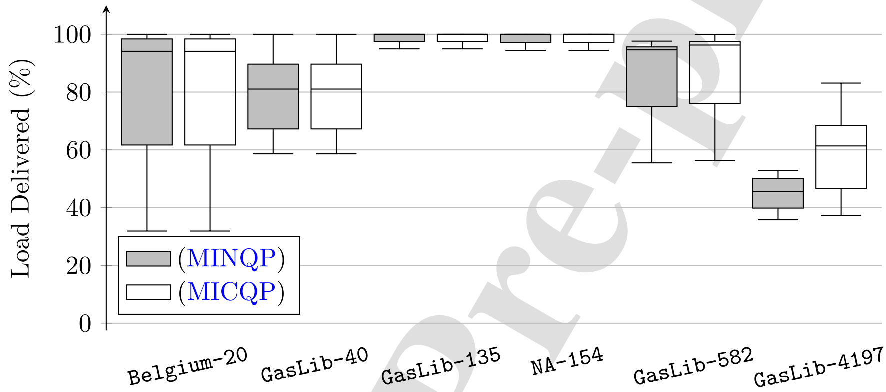

Figure 6: Boxplots of load delivered over earthquake damage scenarios per network, where both the magnitude and epicenter for each scenario are normally distributed. Here, dotted and clear boxplots correspond to (MINQP) and (MICQP) formulations, respectively. Note that each pair of boxplots summarizes only instances solved by *both* (MINQP) and (MICQP).

local magnitude of each earthquake was assumed to be 8.0 with a standard deviation of 0.25, and each mean epicenter was again assumed to be the center of a k-means cluster containing the largest number of junctions, where $k = 5$, and where a distance-based standard deviation of ten kilometers was assumed. Using the models of Campbell (1997) and Lanzano et al. (2014), one thousand random earthquake scenarios were generated per network, where in each, the status per node-connecting component was again determined via a uniform random sampling and comparison with the probability of damage.

Table 5 repeats the format of Table 4 to display aggregate statistics of solver termination statuses across all stochastic earthquake scenarios. For most scenarios, globally optimal solutions to MLD instances were found within the prescribed one hour time limit. For scenarios based on the `GasLib-135`, `GasLib-582`, and `GasLib-4197` networks, however, some instances could not be solved. As in the deterministic scenario analysis, comparing the (MINQP) and (MICQP) formulations shows the benefit of the relaxation-based approach. Furthermore, 133 and one `GasLib-4197` (MINQP) and (MICQP) instances, respectively, were

Network	# Instances	# Feas. (MICQP)	# Feas. (MINQP)	Mean Diff. (%)
`GasLib-11`	1022	1022	1022	0.0
`Belgium-20`	3055	3055	3055	0.1
`GasLib-24`	1051	1051	1051	0.0
`GasLib-40`	3085	3085	3085	11.7
`GasLib-134`	1267	1267	1267	0.2
`GasLib-135`	3305	3305	3305	7.5
`NA-154`	3306	3306	3306	0.0
`GasLib-582`	4233	4233	4233	4.8
`GasLib-4197`	4088	4076	1049	7.9

Table 6: Feasibility statistics for (MICQP) and when integer decisions are fixed within (MINQP). Here, all damage scenarios evaluated in Sections 4.2 through 4.5 are considered.

claimed to be infeasible using default Gurobi parameters. These numbers were, however, reduced to 59 and zero, respectively, when using `NumericFocus=3`.

Figure 6 displays boxplots comparing the proportion of maximum load delivered across all scenarios. Again, the (MINQP) and (MICQP) formulations provide results that are qualitatively similar. The boxplots also show similar differences in vulnerability as those observed in Figure 6. However, the greater variation in epicenters and magnitudes results in greater variation of the effects.

4.6. Feasibility of Relaxation Solutions

The histograms of Section 4.3 (Figure 2) and, to a better extent, the boxplots of Section 4.5 (Figures 5 and 6) highlight that (MICQP) is a relaxation of (MINQP) that *overestimates* the transport capacity of a damaged network. In this section, we further emphasize qualities of the relaxation, showing that although solutions to (MICQP) are often near solutions that are feasible to (MINQP), this is not generally the case. That is, although the *objective* of (MICQP) often provides a good upper bound on the *capacity* of a damaged network, solutions are not necessarily physically feasible, i.e., feasible to (MINQP).

To show this, we revisit all previous damage scenarios studied in Sections 4.2 through 4.5. For each network and scenario, an experiment was performed in which (i) (MICQP) was solved with a one hour time limit, (ii) if available, feasible values of discrete variables, i.e., $\hat{y}$ and $\hat{z}$, were obtained, (iii) the variables y and z of (MINQP) were fixed to $\hat{y}$ and $\hat{z}$, respectively, and (iv) (MINQP) was solved with the fixed discrete variables and a one hour time limit. We remark that y and z were selected for fixing in these experiments because (i) discreteness is a challenging aspect of both (MICQP) and (MINQP) and (ii) fixing values of continuous variables would present difficulties from a numerical perspective.

The second column of Figure 6 lists the number of damage scenarios considered for each network in this set of experiments. The third column lists the number of instances where a solution feasible to (MICQP) was found. The fourth column lists the number of instances where an (MINQP)-feasible solution was found after fixing y and z. The final column lists the mean difference between the objective value of (MICQP) and the partially fixed (MINQP), where

$$\% \text{ Difference} = 100\% \left(\frac{|\hat{\eta}_{(\text{MICQP})} - \hat{\eta}_{(\text{MINQP})}|}{|\hat{\eta}_{(\text{MICQP})}|} \right). \tag{43}$$

It is first remarkable that for all but the largest network, `GasLib-4197`, integer solutions that are feasible to (MICQP) are also always feasible to (MINQP). It is also notable that for the largest network, around a quarter of the integer solutions are feasible to (MINQP). Finally, the mean objective difference is typically small and less than 8%. For cases with relatively large numbers of compressors, there are often larger discrepancies. These results suggest that, for moderately-sized networks where the relaxation is sufficiently tight, solutions may be in close proximity to (MINQP)-feasible solutions. However, they also emphasize that relaxation solutions are, *generally, not physically feasible.*

5. Conclusion

This study introduced the MLD problem for natural gas transmission networks, which seeks to estimate the transport capacity of a damaged gas pipeline network while ensuring the maximal delivery of prioritized load. This task was presented with three successive mathematical programming formulations. First, a mixed-integer nonconvex program was formulated that embeds all physical and engineering requirements for operational feasibility. Second, the first nonconvex program was reformulated *exactly* as a mixed-integer nonconvex quadratic program by introducing new variables. Finally, convex relaxations were applied to all nonconvex relationships in the former problem that involve pressures and mass flows, which resulted in a mixed-integer convex relaxed formulation.

To compare the efficacy of the second and third formulations, a rigorous benchmarking study was conducted over a large number of randomized multi-contingency scenarios on nine networks ranging in size from 11 to 4,197 junctions. First, MLD experiments based on $N-1$ (or single contingency) damage scenarios were conducted. Second, $N-k$ (multi-contingency) damage experiments were performed in order to understand MLD tractability for multimodal failures. A performance comparison of the (MINQP) and (MICQP) formulations was then conducted using results from the $N-1$ and $N-k$ experiments. Finally, a proof-of-concept application based on network damage from a set of synthetically generated earthquakes demonstrated the application of the MLD problem to risk assessment for deterministic and stochastic spatial hazards.

These experimental results lead to three key conclusions. First, the relaxed formulation, (MICQP), provides good bounds on the maximal deliverable load obtained from the full mixed-integer nonconvex formulation, (MINQP). Second, the relaxation-based formulation is more computationally robust than the mixed-integer nonconvex formulation and can solve larger proportions of challenging instances in much shorter amounts of time. Finally, for the largest network (i.e., `GasLib-4197`), the relaxation-based approach begins to show its limitations. For some challenging scenario types (e.g., $N-1$), large numbers of instances cannot be solved because of the relatively larger size of the network.

There are several potential studies that could extend the approaches developed in this study. First, additional relaxation-based methods could be implemented to more accurately and efficiently solve the MLD problem for natural gas networks containing thousands of nodes. To facilitate this, another useful contribution could be the development of new benchmark instances whose sizes range between the sizes of `GasLib-582` and `GasLib-4197`. The origin of numerical instabilities associated with the challenging `GasLib-4197` network, and especially the sources of claimed infeasibility by Gurobi for some (MINQP) instances, should also be thoroughly investigated. This could involve developing new methods for preprocessing network data or nondimensionalizing constraints.

A number of studies could extend the proof-of-concept use cases presented. For example, our MLD approach could be employed within a detailed sensitivity analysis of gas network elements, whereby individual components or combinations of components could be ranked according to their overall effect on total deliverable load. Such an approach could be highly useful in hazard mitigation efforts. Finally, although this study considers steady-state models of the gas network's physics, modeling transient dynamics could be interesting in contingency analysis. The standard definition of MLD in contingency analysis estimates load delivery between (ii) and (iv) of Figure 1 to determine the impact of a contingency. However, it could be interesting to develop a new MLD definition that accounts for the shape and duration of the curve between (i) and (ii). Future studies should strive for greater accuracy while maintaining tractability.

Acknowledgments

The authors express gratitude to Mary Ewers and David Fobes of Los Alamos National Laboratory for their construction of the `NA-154` network model.

Declarations

Funding. The Department of Homeland Security sponsored the production of this material under the U.S. Department of Energy contract for the management and operation of Los Alamos National Laboratory. Los Alamos National Laboratory is operated by Triad National Security, LLC, for the National Nuclear Security Administration of the U.S. Department of Energy (Contract No. 89233218CNA000001).

Availability of Data and Material. `Belgium-20` network data was originally derived from De Wolf & Smeers (2000) and, subsequently, Borraz-Sánchez et al. (2016). Our version of this network data is similar to the `A1` example provided by GasModels. `NA-154` network data is available upon request, subject to approval. `GasLib` network data are publicly available at https://gaslib.zib.de.

Code Availability. The formulations in this paper are implemented in GasModels, publicly available at https://github.com/lanl-ansi/GasModels.jl. The source code for damage scenario preparation and analysis is available upon request, subject to approval.

References

Ahumada-Paras, M., Sundar, K., Bent, R., & Zlotnik, A. (2021). N-k interdiction modeling for natural gas networks. *Electric Power Systems Research*, *190*, 106725. doi:10.1016/j.epsr.2020.106725.

Arya, A. K., & Honwad, S. (2018). Multiobjective optimization of a gas pipeline network: An ant colony approach. *Journal of Petroleum Exploration and Production Technology*, *8*, 1389–1400. doi:10.1007/s13202-017-0410-7.

Atmos International (2021). Atmos Pipe. https://web.archive.org/web/20210512074208/https://www.atmosi.com/us/products-services/atmos-pipe/.

Bent, R., Blumsack, S., Van Hentenryck, P., Borraz-Sánchez, C., & Shahriari, M. (2018). Joint electricity and natural gas transmission planning with endogenous market feedbacks. *IEEE Transactions on Power Systems*, *33*, 6397–6409. doi:10.1109/TPWRS.2018.2849958.

Bent, R., Sundar, K., Fobes, D., Tasseff, B., & Coffrin, C. (2022). GasModels.jl. https://github.com/lanl-ansi/GasModels.jl.

Borraz-Sánchez, C., Bent, R., Backhaus, S., Hijazi, H., & Hentenryck, P. V. (2016). Convex relaxations for gas expansion planning. *INFORMS Journal on Computing*, *28*, 645–656. doi:10.1287/ijoc.2016.0697.

Campbell, K. W. (1997). Empirical near-source attenuation relationships for horizontal and vertical components of peak ground acceleration, peak ground velocity, and pseudo-absolute acceleration response spectra. *Seismological Research Letters*, *68*, 154–179. doi:10.1785/gssrl.68.1.154.

Chen, S., Wei, Z., Sun, G., Wang, D., & Zang, H. (2018). Steady state and transient simulation for electricity-gas integrated energy systems by using convex optimisation. *IET Generation, Transmission & Distribution*, *12*, 2199–2206. doi:10.1049/iet-gtd.2017.1318.

Coffrin, C., Bent, R., Tasseff, B., Sundar, K., & Backhaus, S. (2019). Relaxations of AC maximal load delivery for severe contingency analysis. *IEEE Transactions on Power Systems*, *34*, 1450–1458. doi:10.1109/TPWRS.2018.2876507.

Conti, J., Holtberg, P., Diefenderfer, J., LaRose, A., Turnure, J. T., & Westfall, L. (2016). *International Energy Outlook 2016 with Projections to 2040*. Technical Report U.S. DOE Energy Information Administration (EIA), Washington, D.C.

De Wolf, D., & Smeers, Y. (2000). The gas transmission problem solved by an extension of the simplex algorithm. *Management Science*, *46*, 1454–1465. doi:10.1287/mnsc.46.11.1454.12087.

Dunning, I., Huchette, J., & Lubin, M. (2017). JuMP: A modeling language for mathematical optimization. *SIAM Review*, *59*, 295–320. doi:10.1137/15M1020575.

Energy Solutions (2021). Gas Management Software. https://web.archive.org/web/20210126024052/http://www.energy-solutions.com/products/esi-gas-management-solutions.

ERCOT (2021). Review of February 2021 extreme cold weather event. URL: https://web.archive.org/web/20210319095939/http://www.ercot.com/content/wcm/key_documents_lists/225373/Urgent_Board_of_Directors_Meeting_2-24-2021.pdf.

Gregg Engineering (2021). NextGen Simulation Suite. https://web.archive.org/web/20210516121924/https://www.greggeng.com/software-solutions/nextgen-simulation-suite.

Gugat, M., Leugering, G., Martin, A., Schmidt, M., Sirvent, M., & Wintergerst, D. (2018). MIP-based instantaneous control of mixed-integer PDE-constrained gas transport problems. *Computational Optimization and Applications*, *70*, 267–294. doi:10.1007/s10589-017-9970-1.

Hahn, M., Leyffer, S., & Zavala, V. M. (2017). Mixed-integer PDE-constrained optimal control of gas networks. *Mathematics and Computer Science*, .

Hante, F. M. (2017). Relaxation methods for hyperbolic PDE mixed-integer optimal control problems. *Optimal Control Applications and Methods*, *38*, 1103–1110. doi:10.1002/oca.2315.

Hante, F. M. (2020). Mixed-integer optimal control for PDEs: Relaxation via differential inclusions and applications to gas network optimization. In *Mathematical Modelling, Optimization, Analytic and Numerical Solutions* (pp. 157–171). Singapore: Springer Singapore. doi:10.1007/978-981-15-0928-5_7.

Hiller, B., Koch, T., Schewe, L., Schwarz, R., & Schweiger, J. (2018). A system to evaluate gas network capacities: Concepts and implementation. *European Journal of Operational Research*, *270*, 797–808. doi:10.1016/j.ejor.2018.02.035.

Hoppmann-Baum, K., Hennings, F., Lenz, R., Gotzes, U., Heinecke, N., Spreckelsen, K., & Koch, T. (2021). Optimal operation of transient gas transport networks. *Optimization and Engineering*, *22*, 735–781. doi:10.1007/s11081-020-09584-x.

Koch, T., Hiller, B., Pfetsch, M., & Schewe, L. (2015). *Evaluating Gas Network Capacities*. SIAM.

Lanzano, G., Salzano, E., Santucci de Magistris, F., & Fabbrocino, G. (2014). Seismic vulnerability of gas and liquid buried pipelines. *Journal of Loss Prevention in the Process Industries*, *28*, 72–78. doi:10.1016/j.jlp.2013.03.010. European Process Safety Pioneers.

McCormick, G. P. (1976). Computability of global solutions to factorable nonconvex programs: Part I — Convex underestimating problems. *Mathematical Programming*, *10*, 147–175. doi:10.1007/BF01580665.

Midthun, K. T., Bjorndal, M., & Tomasgard, A. (2009). Modeling optimal economic dispatch and system effects in natural gas networks. *The Energy Journal*, *30*. doi:10.5547/ISSN0195-6574-EJ-Vol30-No4-6.

Misra, S., Vuffray, M., & Chertkov, M. (2015). Maximum throughput problem in dissipative flow networks with application to natural gas systems. arXiv:1504.02370.

Osiadacz, A. (1987). *Simulation and Analysis of Gas Networks*. Gulf Publishing Company, Houston, TX.

PJM Interconnection (2014). *Analysis of Operational Events and Market Impacts During the January 2014 Cold Weather Events*. Technical Report.

Schmidt, M., Aßmann, D., Burlacu, R., Humpola, J., Joormann, I., Kanelakis, N., Koch, T., Oucherif, D., Pfetsch, M. E., Schewe, L., Schwarz, R., & Sirvent, M. (2017). GasLib - a library of gas network instances. *Data*, *2*. doi:10.3390/data2040040.

Schmidt, M., Steinbach, M. C., & Willert, B. M. (2016). High detail stationary optimization models for gas networks: Validation and results. *Optimization and Engineering*, *17*, 437–472. doi:10.1007/s11081-015-9300-3.

Sundar, K., Coffrin, C., Nagarajan, H., & Bent, R. (2018). Probabilistic N-k failure-identification for power systems. *Networks*, *71*, 302–321. doi:10.1002/net.21806.

Wu, F., Nagarajan, H., Zlotnik, A., Sioshansi, R., & Rudkevich, A. M. (2017). Adaptive convex relaxations for gas pipeline network optimization. In *2017 American Control Conference (ACC)* (pp. 4710–4716). doi:10.23919/ACC.2017.7963683.

Zeghadnia, L., Robert, J. L., & Achour, B. (2019). Explicit solutions for turbulent flow friction factor: A review, assessment and approaches classification. *Ain Shams Engineering Journal*, *10*, 243–252. doi:10.1016/j.asej.2018.10.007.

- Maximal Load Delivery (MLD) analysis estimates the capacity of a damaged gas system
- Relaxations of gas network physics increase the tractability of an MLD analysis
- Rigorous benchmarking illustrates computational advantages of the relaxations
- MLD analyses can help estimate the effects of natural disasters on gas networks

All authors have substantively contributed to this manuscript.

Declaration of interests

☒ The authors declare that they have no known competing financial interests or personal relationships that could have appeared to influence the work reported in this paper.

☐ The authors declare the following financial interests/personal relationships which may be considered as potential competing interests: